



HAL
open science

A common mechanism of Sec61 translocon inhibition by small molecules

Samuel Itskanov, Laurie Wang, Tina Junne, Rumi Sherriff, Li Xiao, Nicolas Blanchard, Wei Shi, Craig Forsyth, Dominic Hoepfner, Martin Spiess, et al.

► **To cite this version:**

Samuel Itskanov, Laurie Wang, Tina Junne, Rumi Sherriff, Li Xiao, et al.. A common mechanism of Sec61 translocon inhibition by small molecules. *Nature Chemical Biology*, 2023, 19 (9), pp.1063-1071. 10.1038/s41589-023-01337-y . hal-04262928

HAL Id: hal-04262928

<https://hal.science/hal-04262928>

Submitted on 31 Oct 2023

HAL is a multi-disciplinary open access archive for the deposit and dissemination of scientific research documents, whether they are published or not. The documents may come from teaching and research institutions in France or abroad, or from public or private research centers.

L'archive ouverte pluridisciplinaire **HAL**, est destinée au dépôt et à la diffusion de documents scientifiques de niveau recherche, publiés ou non, émanant des établissements d'enseignement et de recherche français ou étrangers, des laboratoires publics ou privés.

16 **A common mechanism of Sec61 translocon inhibition by small molecules**

17

18 Samuel Itskanov^{1,#}, Laurie Wang^{2,#}, Tina Junne³, Rumi Sherriff², Li Xiao⁴, Nicolas Blanchard⁵,
19 Wei Q. Shi⁶, Craig Forsyth⁴, Dominic Hoepfner⁷, Martin Spiess³, and Eunyong Park^{2,8}

20

21 ¹Biophysics Graduate Program, University of California, Berkeley, Berkeley, CA 94720, USA.

22 ²Department of Molecular and Cell Biology, University of California, Berkeley, CA 94720, USA.

23 ³Biozentrum, University of Basel, CH-4056 Basel, Switzerland.

24 ⁴Department of Chemistry and Biochemistry, The Ohio State University, Columbus, Ohio 43210,
25 United States.

26 ⁵Université de Haute-Alsace, Université de Strasbourg, CNRS, LIMA, UMR 7042, 68000
27 Mulhouse, France.

28 ⁶Department of Chemistry, Ball State University, Muncie, IN 47306, USA.

29 ⁷Novartis Institutes for BioMedical Research, Novartis Pharma AG, Forum 1 Novartis Campus,
30 CH-4056 Basel, Switzerland

31 ⁸California Institute for Quantitative Biosciences, University of California, Berkeley, CA 94720,
32 USA.

33 These authors contributed equally: Samuel Itskanov and Laurie Wang

34 Corresponding author: Eunyong Park (e-mail: eunyong_park@berkeley.edu)

35

36 **Abstract**

37 The Sec61 complex forms a protein-conducting channel in the endoplasmic reticulum
38 membrane that is required for secretion of soluble proteins and production of many membrane
39 proteins. Several natural and synthetic small molecules specifically inhibit Sec61, generating
40 cellular effects that are useful for therapeutic purposes, but their inhibitory mechanisms remain
41 unclear. Here we present near-atomic-resolution structures of human Sec61 inhibited by a
42 comprehensive panel of structurally distinct small molecules—cotransin, decatransin, apratoxin,
43 ipomoeassin, mycolactone, cyclotriazadisulfonamide, and eeyarestatin. All inhibitors bind to a
44 common lipid-exposed pocket formed by the partially open lateral gate and plug domain of
45 Sec61. Mutations conferring resistance to the inhibitors are clustered at this binding pocket. The
46 structures indicate that Sec61 inhibitors stabilize the plug domain in a closed state, thereby
47 preventing the protein-translocation pore from opening. Our study provides the atomic details of
48 Sec61–inhibitor interactions and the structural framework for further pharmacological studies
49 and drug design.

50 (150 words)

51

52 Introduction

53 The universally conserved heterotrimeric Sec61 complex (SecY in prokaryotes) plays essential
54 roles in biosynthesis of more than one third of proteins in all species (for recent review, see ref.
55 ¹). In eukaryotes, secretory proteins are first translocated into the endoplasmic reticulum (ER) by
56 the Sec61 complex before reaching the cell surface by vesicular trafficking. The Sec61 complex
57 also mediates membrane integration of many proteins, including most cell surface receptors and
58 cell adhesion molecules. The Sec61/SecY channel has an hourglass-like structure with a pore
59 constriction (termed the pore ring) halfway across the membrane, which is gated by a
60 movement of a plug-like ER-luminal (or extracellular in SecY) domain of the channel². In
61 addition, the channel has a seam (lateral gate) in the wall that can open laterally in the plane of
62 the membrane to release transmembrane segments (TMs) of membrane protein clients into the
63 lipid phase. Concerted opening of the luminal and lateral gates is also required for initial
64 insertion of the client protein's hydrophobic signal sequence or uncleavable signal anchor into
65 the channel (Fig. 1a).

66 The Sec61/SecY channel translocates polypeptides either co-translationally by docking a
67 translating ribosome or post-translationally by engaging a fully synthesized polypeptide client. In
68 eukaryotes, the post-translational mode is enabled by association of the channel with two
69 additional membrane proteins Sec63 and Sec62 (ref. ^{3,4}). X-ray crystallography and cryo-
70 electron microscopy (cryo-EM) have visualized structures of the Sec61/SecY channel in
71 different functional states and revealed how it is gated and engages with client proteins^{2,5-14}. The
72 current model posits that association of a ribosome or Sec63 slightly perturbs ("primes") or
73 partially opens the lateral gate^{7,11,12} (Fig. 1a). Insertion of the client polypeptide needs further
74 widening of the lateral opening and a displacement of the plug away from the pore, which occur
75 in a cooperative manner. In cotranslational translocation, these conformational changes are
76 presumed to be induced by an interaction between the channel and the signal
77 sequence/anchor^{7,9}, whereas in post-translational translocation, they seem to be mediated by
78 Sec62¹³.

79 Several natural and synthetic small molecules bind to Sec61 and inhibit protein translocation
80 (for review, see ref. ^{15,16}). These inhibitors have been investigated as potential anticancer,
81 antiviral, and/or immunosuppressive agents¹⁷⁻²⁰. Inhibition of Sec61 leads to downregulation of
82 disease-related and clinically-relevant proteins, such as cytokines, cell surface receptors, and
83 viral membrane proteins. Indeed, one such Sec61 inhibitor is currently being tested in a phase-I
84 clinical trial for treatment of solid tumor malignancies²¹. A founding class of Sec61 inhibitors is a
85 group of fungal-derived cyclic heptadepsipeptides named cotransins²²⁻²⁴. Other naturally
86 occurring inhibitors discovered to date are decatransin, mycolactone, apratoxins, coibamide A,
87 and ipomoeassin F, which are produced by certain fungal, bacterial, and plant species²⁵⁻³⁰. In
88 addition, two synthetic compounds cyclotriazadisulfonamide (CADA) and eeyarestatin I (ESI)
89 have also been shown to inhibit the Sec61 channel^{31,32}. These inhibitors are structurally
90 unrelated to each other, but several of them have been suggested to bind to an overlapping site
91 in the Sec61 channel based on their abilities to compete for Sec61 binding. Remarkably,
92 cotransin and CADA inhibit Sec61 in a client-specific manner^{22,23,33}, whereas other inhibitors act
93 more broadly independent of clients. Biochemical data suggest that cotransin likely interacts
94 with the lateral gate and/or the plug of Sec61 (ref. ³⁴). However, key information regarding the

95 actions of these inhibitors remains unavailable, including molecular details about Sec61-inhibitor
96 interactions, which specific steps along the translocation process are inhibited, and what
97 underlies client-specific versus broad-spectrum inhibition. This has limited our capability to
98 design or discover additional therapeutically promising small-molecule agents that target Sec61.

99

100 **Results**

101 **Cryo-EM analysis of inhibitor-bound Sec61**

102 To understand the mechanism of Sec61 inhibition, we sought to determine high-resolution
103 structures of inhibitor-bound Sec61 using cryo-EM. To date, all mammalian Sec61 structures
104 have been obtained from ribosome-bound cotranslational complexes^{7,8}. However, due to the
105 flexibility of Sec61 with respect to the ribosome, this approach limits the resolution of Sec61 to
106 only ~5 Å, a resolution that is impractical to model protein side chains and small ligands⁷. This
107 limitation is also apparent in the recent cryo-EM structures of the Sec61-ribosome complex
108 treated with mycolactone³⁵, a cotransin derivative (KZR-8445)³⁶, or a CADA derivative
109 (CK147)³⁷. By contrast, we previously attained 3.1–3.7-Å resolution structures of the Sec61
110 channel from fungal post-translational translocation complexes^{11,13} (termed the Sec complex),
111 which contained Sec62, Sec63 and fungal-specific nonessential Sec71 and Sec72 in addition to
112 the three (α , β , and γ) subunits of the Sec61 complex. Thus, we reasoned that use of the Sec
113 complex would be an effective approach to study Sec61 inhibitors.

114 To enable high-resolution cryo-EM analysis of inhibitor-bound human Sec61, we designed a
115 chimeric Sec complex, whose transmembrane and cytosolic domains are derived from the
116 human and yeast proteins, respectively (Fig. 1b). Our initial efforts employing the entirely yeast
117 or human Sec complex were unsuccessful. The yeast Sec complex incubated with cotransin
118 ‘compound 2’ (hereafter referred to as cotransin CP2)²⁵ did not show any cotransin-like feature
119 in the cryo-EM map (Extended Data Fig. 1 a and b). This could be due to a lower binding affinity
120 of cotransin CP2 towards yeast Sec61 compared to mammalian Sec61²⁵, the presence of
121 detergent in the sample, or both. We could see a putative cotransin CP2 density in a cryo-EM
122 structure of the human Sec complex lacking Sec62, but the resolution could not be improved
123 beyond ~5 Å, probably due to high flexibility of the cytosolic domain of human Sec63 (Extended
124 Data Fig. 1 c–f). We hypothesized that the resolution could be improved by replacing the
125 cytosolic domain of Sec63 in the human complex with the yeast counterpart, as yeast Sec63,
126 along with additional Sec71–Sec72 proteins, consistently showed well-defined features in our
127 previous cryo-EM studies^{11,13}. While this chimeric construct would not be functional for post-
128 translational translocation without a matching chimeric Sec62 subunit that can interact with both
129 human Sec61 and yeast Sec63, we expected that inhibitors would still bind efficiently to the
130 channel as the Sec61 sequence is mostly human.

131 The human-yeast chimeric Sec complex reconstituted into a peptidisc³⁸ indeed yielded
132 dramatically improved structures at overall 2.5 to 2.9-Å resolution with most side-chain densities
133 well defined (Fig 1c, and Extended Data Figs. 2–4 and Supplementary Table 1). In the absence
134 of inhibitors, particle images could be sorted into two three-dimensional (3-D) classes with minor
135 differences (Extended Data Fig. 2 b–h). In both classes, the Sec61 channel adopts a similar

136 conformation, including a partially open lateral gate and a closed plug, as expected for a
137 complex lacking Sec62 (ref. ¹³). However, the two classes showed slightly different
138 arrangements of Sec61 with respect to Sec63-Sec71-Sec72 due to a loose contact between the
139 engineered L6/7 loop of Sec61 α and the FN3 domain of yeast Sec63 in Class 2 (Extended Data
140 Fig. 2 g and h).

141 For inhibitor-bound structures, we used five naturally occurring inhibitors, cotransin CP2,
142 decatransin, apratoxin F, ipomoeassin F, and mycolactone; and two designed synthetic
143 compounds CADA and ESI. Focused refinement masking out the cytosolic domains of Sec63-
144 Sec71-Sec72 further improved the map of the Sec61 complex (at overall resolution of 2.6 to 3.2
145 Å) showing clear, well-defined density features for the added inhibitor (Fig. 1 d–k, Extended
146 Data Figs. 3 and 4, and Supplementary Table 2). Local resolution around the inhibitor-binding
147 region was on par with or better than the overall resolution owing to relatively uniform resolution
148 distributions (Extended Data Fig. 3f). Reliable atomic models of inhibitor molecules could be
149 built into the densities of inhibitors based on their two-dimensional (2-D) chemical structures
150 (Fig. 1 d–k). However, we note that positions and orientations of certain atoms and bonds may
151 deviate from their true structures as our structures do not resolve individual atoms. When we
152 compared the cotransin CP2-bound Sec61 structures from the human and chimeric Sec
153 complexes, the two structures were essentially superimposable (Extended Data Fig. 5). This
154 suggests that the Sec61 channel in the chimeric complex can adopt the conformations that are
155 compatible with inhibitor binding observed in the human Sec complex.

156

157 Inhibitor-binding site

158 Despite their diverse chemical structures, all analyzed inhibitors are found to bind essentially to
159 the same site in the Sec61 channel (Figs. 1 and 2 a–c, and Extended Data Fig. 6). The pocket
160 is formed at the partially open lateral gate, approximately halfway across the membrane. The
161 inhibitors commonly interact with lateral gate helices TMs 2b, 3, and 7 of the Sec61 α subunit.
162 However, it should be noted that the actual structure of the pocket substantially varies
163 depending on the bound inhibitor because the lateral gate adopts different degrees of opening
164 (Fig. 2d, and Extended Data Fig. 6). The width of the lateral gate opening is widest in the
165 cotransin CP2-bound structure and narrowest in the ipomoeassin F-bound structure. During
166 protein translocation, the lateral gate of the Sec61/SecY channel dynamically adopts closed or
167 variable open states by a relative motion between the N- and C- terminal halves of the α
168 subunit^{2,5-14}. Our structures show that inhibitors bind to the lateral gate in one of these partially
169 open states facilitated by the conformational flexibility of Sec61 and form a tight fit with the
170 pocket. A notable example of such flexibility can be seen in the ipomoeassin F-bound structure,
171 where the inhibitor binding even caused partial dissociation of Sec61 from Sec63 to
172 accommodate a near-closed conformation of the lateral gate (Extended Data Fig. 7). Compared
173 to natural inhibitors, the interfaces of CADA and ESI to Sec61 seem less extensive, possibly
174 explaining the lower (micromolar-range) affinities of these synthetic inhibitors (Extended Data
175 Fig. 6).

176 In addition to the lateral gate, the plug and pore ring critically participate in binding of all
177 inhibitors. The partially open lateral gate of inhibited Sec61 is reminiscent of conformations
178 observed with substrate-engaged Sec61. In fact, the inhibitor binding site largely coincides with
179 where a signal sequence docks upon the insertion of a substrate protein into the channel^{9,10}.
180 However, one crucial difference exists between polypeptide substrates and inhibitors: unlike the
181 signal sequence, all inhibitors also form a direct contact with the plug in a closed position
182 through hydrophobic moieties (Figs. 1 and 3). Many inhibitors even further intercalate into the
183 dilated, crescent-shaped pore ring and interact with pore-ring residues (Ile81, Val85, Ile179,
184 Ile183, Ile292, and/or Ile449). In the cases of mycolactone and ESI, their extended chain
185 penetrates deeply into the channel interior and occupies a substantial space of the channel's
186 cytosolic funnel (Fig. 3 and Extended Data Figs. 6 and 8). These parts of mycolactone and ESI
187 are known to be critical for their inhibitory activity^{17,32}.

188

189 **Structures of inhibitors and their interactions with Sec61**

190 Except for cotransin and apratoxin, the structures of which were determined in organic solvents
191 by NMR spectroscopy or X-ray crystallography^{39,40}, 3D structures of most Sec61 inhibitors were
192 unknown. Our cryo-EM structures now reveal their 3D structures in association with the Sec61
193 channel. Notably, conformations of cotransin CP2 and apratoxin F in our cryo-EM structures are
194 highly similar to those structures determined in organic solvent^{39,40}. This might be because the
195 inhibitor-binding site in Sec61 forms a markedly hydrophobic environment. Particularly, the
196 pocket is open towards the lipid phase (Figs. 1 and 2), and thus, all inhibitors are expected to
197 interact with hydrocarbon tails of membrane lipids. The lipid-exposed parts of inhibitors are
198 predominantly hydrophobic (Fig. 3). Similarly, the parts of inhibitors that face the Sec61 channel
199 are mostly hydrophobic as they form contacts with hydrophobic side chains from the lateral
200 gate, plug, and pore ring of Sec61 α .

201 While van der Waals interactions between apolar groups of inhibitors and Sec61 seem to be
202 dominant contributors to inhibitor binding, our cryo-EM structures also show a recurring pattern
203 of polar interactions between Sec61 and inhibitors. In the closed channel, the lateral gate
204 contains a conserved polar cluster halfway across the membrane, formed mainly by the side
205 chain amide groups of Gln127 (Q127) in TM3 and Asn300 (N300) in TM7. Mutations in this
206 polar cluster has been shown to affect the energetics of channel gating⁴¹. In the inhibitor-bound
207 structures, Q127 and N300 are separated by lateral gate opening, but instead they do form
208 polar interactions with certain oxygen and nitrogen atoms in the backbones of the inhibitors.
209 Given that these prong-like polar interactions are present in a predominantly hydrophobic milieu,
210 it is likely that they substantially strengthen inhibitor binding at the pocket (see below).

211

212 **Mutations in Sec61 conferring resistance to inhibitors**

213 Several point mutations in Sec61 α have been found to confer resistance to Sec61
214 inhibitors^{25,26,28-30,34,35}. These mutations are mostly located in the plug and the lateral gate. Given
215 the direct interactions between inhibitors and these parts, disruption of the inhibitor binding

216 surface could be a mechanism for these mutations. However, it has also been proposed that
217 mutations might work indirectly through altering the conformation of the channel³⁵. Extensive
218 biochemical studies of the Sec61/SecY complexes have well established that mutations in the
219 lateral gate, plug, and pore ring often change the gating behavior of the channel⁴¹⁻⁴³. The best-
220 known examples are *prl* mutations that give rise to relaxed client selectivity through increased
221 propensity of channel opening. Thus, this phenotypic complexity has obscured how Sec61
222 mutations confer resistance to inhibitors. Moreover, positions of the identified mutations were
223 often redundant and sparse, limiting detailed investigation of their mechanisms.

224 To biochemically probe inhibitor-binding sites in the Sec61 complex, we conducted a
225 comprehensive mutational analysis fully blinded from our cryo-EM study. We focused on two
226 inhibitors cotransin CP2 and ipomoeassin F, which were readily available to us. In addition to
227 anti-proliferation activities on mammalian cancer cell lines, these compounds also cause growth
228 retardation of yeast cells in a Sec61 α (Sec61p)-specific manner²⁵. Therefore, we tested 84 point
229 mutations on 34 amino acid positions in yeast Sec61 α for their half-maximal growth inhibitory
230 concentration (IC₅₀) (Supplementary Table 3). Positions were mainly chosen from the cytosolic
231 funnel and lateral gate as they were likely candidates to bind inhibitors (each site was typically
232 mutated to either Asp or Trp). This led us to identify 19 and 14 new resistance-conferring
233 positions for cotransin CP2 and ipomoeassin F, respectively.

234 We then mapped the mutation positions onto the cryo-EM structures. The results clearly show
235 that most resistance mutations are clustered around bound cotransin CP2 or ipomoeassin F
236 (Figure 4 a and b), suggesting that their primary mechanism is through directly impairing the
237 inhibitor-binding surface. However, some mutations (e.g., mutations equivalent to R66I/G and
238 E78K in human Sec61 α) are located at distal sites in the plug, and they may act through a
239 conformational change in the plug domain. The plug makes a substantial contact with all tested
240 inhibitors and is one of the most mobile parts of Sec61. Thus, altered structure or dynamics of
241 the plug may explain the weakened inhibitor binding.

242 Lastly, we investigated the importance of polar interactions at the binding site by mutational
243 analysis. In the yeast growth assay, we found that an N302L mutation in yeast Sec61 α
244 (equivalent to N300L in human Sec61 α) confers strong resistance to cotransin CP2,
245 deca-transin, and ipomoeassin F (Fig. 4 c–e). A Q129L mutant (equivalent to Q127L in human
246 Sec61 α) showed strong to intermediate resistance to deca-transin and ipomoeassin F and mild
247 effects on cotransin CP2. We further tested the effects of Q127 and N300 mutations on
248 inhibition using human cells because several inhibitors exerted little or no effects on yeast
249 growth even at high concentrations (200 μ M for mycolactone and apratoxin F; and 1 mM for
250 CADA and ESI). We generated stable HEK293 cell lines that overexpress Sec61 α (Extended
251 Data Fig. 9). All natural-product inhibitors potently inhibited cell viability at nano- or subnano-
252 molar concentrations in wild-type expressing cells (Fig. 4 f–j). Similar to the yeast-based assay,
253 expression of Q127A or N300A mutant Sec61 α markedly shifted dose-response curves to
254 higher inhibitor concentrations, suggesting that the mutations substantially decrease inhibitor-
255 binding affinities. Unlike natural inhibitors, we could not observe Sec61-dependent cytotoxicity in
256 the cell-based assay from synthetic designed inhibitors CADA and ESI. However, CADA
257 inhibited expression of human CD4 with an IC₅₀ of 0.6 μ M, similar to previous report³¹, and the
258 Q127A and N300A mutations substantially reduced the inhibition by CADA (Fig. 4k and

259 [Extended Data Fig. 9](#)). In all these experiments, the N300 mutations generally led to stronger
260 resistance than the Q127 mutations. This might be explained in part by the structural
261 observation that the side-chain amide of N300 more directly faces toward the inhibitors
262 compared to Q127 ([Extended Data Fig. 8](#)).

263

264 **Discussion**

265 Our study reveals how Sec61 inhibitors interact with the channel and block the protein
266 translocation. Remarkably, all seven tested inhibitors were found to bind to the same site in the
267 channel formed by a partially open lateral gate and the fully closed plug domain, suggesting that
268 this mode of interaction provides possibly the most effective mechanism for small molecules to
269 inhibit the Sec61 channel. Among all known major Sec61 inhibitors to date, coibamide A is the
270 only compound that was not included in the present study. However, given the previous
271 observations that it competes with apratoxin A and mycolactone for Sec61 binding and that its
272 resistant mutation could be found also in the plug³⁰, coibamide A is likely to bind to the same or
273 an overlapping site. We note that the mycolactone and CADA derivative CK147 models
274 proposed in the recent medium-resolution cryo-EM studies^{35,37} using ribosome-bound Sec61
275 fundamentally differ in both position and conformation from those we found in our study
276 ([Extended Data Fig. 10](#)). Although the mycolactone (PDB 6Z3T) and CK147 (PDB 8B6C)
277 models in these studies might represent alternative binding modes, understanding of these
278 discrepancies would require further investigation, such as high-resolution cryo-EM analysis of
279 inhibited cotranslational complexes. We also note the KZR-8445-bound Sec61 structure³⁶ and
280 our cotransin CP2-bound structure show some differences. While the overall conformation of
281 the channel and the location of the binding pocket seem consistent, the orientation of the KZR-
282 8445 model is different from that of cotransin CP2 in our study. This discrepancy is more likely
283 due to a limited map resolution of the ribosome–Sec61–KZR-8445 structure, although we
284 cannot rule out a possibility that it may originate from minor structural differences between the
285 two cotransin compounds.

286 Despite distinct chemical structures of the inhibitors, some common features among them could
287 be inferred from our results. First, the inhibitors have two major clusters of hydrophobic
288 moieties, one arranged to interact with the plug and the lateral gate, and the other with
289 membrane lipids. The Sec61-facing sides are characterized by strong surface complementarity
290 for the binding pocket, while the lipophilicity of the other parts would also contribute to efficient
291 binding as the pocket exists within the plane of the membrane. Second, all inhibitors form polar
292 interactions between their backbone and the side chains of the lateral gate (mainly N300 and
293 Q127 of Sec61 α). We found that this is crucial for Sec61 binding affinity. These polar groups of
294 inhibitors would also provide some water solubility of the compounds. Third, certain inhibitors,
295 such as mycolactone and ESI, further penetrate the cytosolic funnel of Sec61 forming additional
296 polar and hydrophobic interactions therein. These interactions likely contribute to the binding
297 energy of the inhibitor and their broad-spectrum activity.

298 Our data indicate that all known Sec61 inhibitors block the protein translocation process
299 commonly by locking both lateral and luminal gates of Sec61 into translocation-incompetent

300 conformations (Fig. 5a). Although the lateral gate stays partially open, it does not provide
301 sufficient space for a signal sequence/anchor to pass. Importantly, the luminal gate, i.e., the
302 plug, remains fully closed such that the client polypeptide cannot insert into the pore. Overall, all
303 three key gating elements—the lateral gate, plug, and pore ring—are cemented together by the
304 inhibitor at their interface, thereby prohibiting their concerted opening required for the client
305 protein insertion.

306 Although further investigations would be necessary, our comparative analysis also hints at why
307 certain inhibitors exhibit client-dependent translocation inhibition. Cotransin and CADA have
308 been shown to be less effective in blocking translocation of client proteins containing a stronger
309 targeting signal, such as a signal sequence with higher hydrophobicity or a TM signal
310 anchor^{44,45}. Our structures show that in the cotransin CP2-bound structure, the lateral gate
311 adopts a relatively more open conformation on the cytosolic side (Fig. 2). This may allow certain
312 hydrophobic interactions between the lateral gate and the incoming signal sequence/anchor
313 (Fig. 5b). A stronger interaction exerted by a stronger targeting signal probably tends to further
314 pry open the lateral gate, promoting the inhibitor to be released. Although the lateral gate of the
315 CADA-bound structure is not as wide as that of cotransin CP2-bound Sec61, its relatively low
316 binding affinity (~0.2–2 μM) might facilitate certain hydrophobic signals to overcome inhibition.
317 On the other hand, those inhibitors that deeply insert into the pore and cytosolic funnel of the
318 channel, such as mycolactone and ESI, may tend to exert broad-spectrum inhibition by
319 additionally impeding client insertion into the pore.

320 It remains unclear whether binding of an inhibitor requires prior opening of the Sec61 channel.
321 In our chimeric complex, the lateral gate is partially opened by Sec63. In co-translational
322 translocation, it has been generally thought that the ribosome docking alone does not open the
323 lateral gate to a considerable extent⁷, which seems necessary for inhibitor binding. However, a
324 transient breathing motion of the channel might allow inhibitors to bind. Single-molecule
325 fluorescence studies of the bacterial SecY channel have indicated that the lateral gate
326 spontaneously fluctuates between closed and open states without any binding partner^{46,47}.
327 Thus, it is possible that inhibitor binding may not require priming or partial opening of the
328 channel induced allosterically by the ribosome or Sec63.

329 It is also unclear how inhibitors affect other functions of the Sec61 channel beyond its role in
330 protein translocation. Previous studies have reported that the Sec61 channel is responsible for
331 passive calcium leakage from the ER lumen and that certain Sec61 inhibitors, such as
332 mycolactone and ESI, enhance this leak^{48,49}. Although our current data do not provide structural
333 insight into calcium permeation by Sec61, it is possible that some relevant conformations for this
334 activity were not captured in our analysis. It is also possible that the calcium leakage involves
335 other translocon components that are absent in our study. Given the importance of calcium in
336 the physiology of metazoan cells, these outstanding issues warrant further study.

337 Lastly, the rich structural and mechanistic knowledge we provide here can facilitate structure-
338 guided design of Sec61 inhibitors. The Sec61 channel has been considered as a promising
339 target for therapeutic intervention due to its essential role in production of many cytokines,
340 surface receptors, and cell adhesion molecules that are clinically relevant. Nevertheless,
341 currently available Sec61 inhibitors would need further structural optimizations to improve their

342 effectiveness and pharmacological properties while reducing undesired cytotoxicity. Our new
343 approach enabling high-resolution structural analysis of human Sec61 and bound ligands would
344 accelerate efforts to understand the mechanisms of new Sec61 inhibitors and optimize
345 previously identified molecules.

346

347 **Acknowledgments**

348 We thank Dan Toso for support for electron microscope operation, Guanghui Zong for
349 ipomoeassin F synthesis, Philippe Mathys and Ralph Riedl for help acquiring the IC₅₀ data. E.P.
350 was supported by the Vallee Scholars Program, Pew Biomedical Scholars Program, and
351 Hellman Fellowship. S.I. and L.W. were supported by a National Institutes of Health training
352 grant (5T32GM008295). M.S and T.J. were supported by the Swiss National Science
353 Foundation (31003A-182519). N.B was supported by Fondation Raoul Follereau and Fondation
354 Pour Le Développement De La Chimie Des Substances Naturelles Et Ses Applications. W.Q.S.
355 (synthesis of ipomoeassin F) was supported by an AREA grant from National Institutes of
356 Health (GM116032). C.F. and L.X. were supported by the Ohio State University.

357

358 **Author contributions**

359 E.P. conceived the project and supervised the cryo-EM study. L.W. and S.I. cloned the chimeric
360 Sec construct and prepared protein samples. S.I., L.W., and E.P. collected and analyzed cryo-
361 EM data and built atomic models. L.W. performed the human cell-based assays. R.S. helped
362 purification of the human Sec complex and cloning of the chimeric Sec complex. T.J., M.S., and
363 D.H. performed the yeast mutational study. D.H. provided cotransin CP2 and decatransin. C.F.
364 and L.X. provided apratoxin F. W.S. provided ipomoeassin F. N.B. provided mycolactone. All
365 authored contributed to interpret results. E.P. wrote the manuscript with input from all authors.

366

367 **Competing interests**

368 During the revision of the manuscript, the Park lab (E.P. and L.W.) signed a sponsored research
369 collaboration agreement with Kezar Life Sciences. The remaining authors declare no competing
370 interests.

371

372 **Figure legends**

373 **Figure 1. Cryo-EM structures of the human Sec61 complex inhibited by various small-**
374 **molecule inhibitors. a**, Architecture of the Sec61 channel and overall model for gating and
375 substrate engagement. **b**, Design of a human-yeast chimeric Sec complex. Parts derived from
376 human and yeast proteins are outlined with solid and dashed lines, respectively. Note that
377 except for the cytosolic L6/7 and L8/9 loops, Sec61 α is from the human SEC61A1 protein
378 sequence. Hs, *Homo sapiens*; Sc, *Saccharomyces cerevisiae*; J, J-domain. **c**, 2.7-Å-resolution
379 cryo-EM map of the chimeric Sec complex in an apo state (Class 1, unsharpened map). The
380 lateral gate helices are indicated by dashed lines and TM numbers. The region outlined by a
381 rectangle indicates the inhibitor-binding site (also see **d–k**). **d–k**, Views into the inhibitor-binding
382 site of Sec61 α of apo and inhibitor-bound structures. Cryo-EM maps (semi-transparent surface)
383 and atomic models were overlaid. Inhibitor and plug densities are shown in cyan and purple,
384 respectively. Dashed lines indicate lateral gate helices TMs 2b, 3, and 7 as in c.

385

386 **Figure 2. Structural plasticity of the inhibitor-binding pocket. a–c**, The inhibitor-binding
387 pocket of Sec61 and bound inhibitors are shown in surface (protein) and sphere (inhibitors)
388 representations. Shown are for cotransin CP2 (a), decatransin (b), and ipomoeassin F (c). For
389 other inhibitors, see [Extended Data Fig. 6](#). Conserved polar amino acids N300 and Q127 at the
390 inhibitor binding site (also see Fig. 3) are indicated in light and dark orange, respectively. Note
391 that part (cinnamate moiety) of ipomoeassin is deeply buried inside the channel and invisible in
392 this representation. **d**, Superposition of the Sec61 structures bound to cotransin CP2 (red),
393 decatransin (green), and ipomoeassin F (pink). Note differences in the lateral gate opening due
394 to the varying position of the N-terminal half of Sec61 α , particularly TMs 2b and 3.

395

396 **Figure 3. Maps for interactions between Sec61 and inhibitors. a**, The chemical structure of
397 cotransin CP2 and the positions of amino acids (ovals) of Sec61 in the immediate vicinity are
398 drawn in a two-dimensional representation. Different colors were used for ovals to indicate
399 regions in Sec61 α : purple–plug, brown–pore ring, gray–lateral gate, light and dark oranges–
400 polar cluster Q127/N300, and white–others. In the cotransin CP2 chemical structure, main lipid-
401 exposed parts are in green whereas channel-facing parts are in blue. Moieties in orange and
402 red interact with N300 and Q127 respectively. **b–g**, As in a, but drawn for decatransin (b),
403 apratoxin F (c), mycolactone (d), ipomoeassin F (e), CADA (f), and ESI (g). Dashed lines
404 indicate putative hydrogen bonds. Note that in the mycolactone-bound structure, a water
405 molecule coordinated by Sec61 and mycolactone was observed in the pocket. For 3D
406 structures, see [Extended Data Fig. 8](#).

407

408 **Figure 4. Inhibitor-resistant mutations. a**, Positions of mutations tested with yeast Sec61
409 were mapped onto the cotransin CP2-bound structure (also see [Supplementary Table 3](#)). Left,
410 front view; right, cutaway side view. Cotransin CP2 (cyan) and amino acid side chains are
411 shown as spheres. Red and pale green spheres indicate positions in which mutation to Asp or

412 Trp develops high and no cotransin CP2 resistance, respective. Magenta, positions of other
413 resistant mutations previously reported^{25,34}. **b**, As in a, but with ipomoeassin-F-resistant
414 mutations. Yellow spheres additionally show positions that give rise to moderate ipomoeassin F
415 resistance. **c–e**, Effects of Sec61 lateral gate polar amino acid mutations on yeast growth
416 inhibition by cotransin CP2, dectransin, and ipomoeassin F (residue numbers are according to
417 yeast Sec61). Shown are means, s.e.m., and fitted curves (n=3 independent experiments for
418 cotransin CP2 and dectransin; n=4 independent experiments for ipomoeassin F). **f–j**, Dose-
419 response curves for indicated inhibitors from viability assays of cultured human (HEK293) cells
420 expressing the indicated Sec61 α variant (residue numbers are according to human SEC61A1;
421 means and s.e.m., n=4 independent experiments). **k**, Inhibition of expression of CD4 in HEK293
422 by CADA (means and s.e.m., n=4 independent experiments).

423

424 **Figure 5. Proposed model for Sec61 inhibition.** **a**, General model for the mechanism of
425 Sec61 inhibitors. Inhibitors bind to Sec61 in a partially open conformation and preclude the plug
426 from opening. This prevents substrate polypeptide insertion. **b**, A proposed model for client-
427 specific inhibition. Certain client-specific inhibitors may allow an interaction between strong
428 signals (e.g., TM signal anchors) and the channel such that the signal sequence/anchor is
429 wedged into the partially open lateral gate. This would further open the lateral gate to cause
430 release of the inhibitor. Inhibitors forming less interactions with the pore and plug, rendering the
431 lateral gate into a more open conformation, and/or displaying a weaker overall affinity are likely
432 to be overcome by this manner.

433

434

435 **References**

- 436 1 Itskanov, S. *et al.* Mechanism of Protein Translocation by the Sec61 Translocon Complex. *Cold*
437 *Spring Harb Perspect Biol* (2022).
- 438 2 Van den Berg, B. *et al.* X-ray structure of a protein-conducting channel. *Nature* **427**, 36-44
439 (2004).
- 440 3 Deshaies, R. J. *et al.* Assembly of yeast Sec proteins involved in translocation into the
441 endoplasmic reticulum into a membrane-bound multisubunit complex. *Nature* **349**, 806-808
442 (1991).
- 443 4 Panzner, S. *et al.* Posttranslational protein transport in yeast reconstituted with a purified
444 complex of Sec proteins and Kar2p. *Cell* **81**, 561-570 (1995).
- 445 5 Egea, P. F. *et al.* Lateral opening of a translocon upon entry of protein suggests the mechanism
446 of insertion into membranes. *Proc Natl Acad Sci U S A* **107**, 17182-17187 (2010).
- 447 6 Park, E. *et al.* Structure of the SecY channel during initiation of protein translocation. *Nature*
448 **506**, 102-106 (2014).
- 449 7 Voorhees, R. M. *et al.* Structure of the mammalian ribosome-Sec61 complex to 3.4 Å resolution.
450 *Cell* **157**, 1632-1643 (2014).
- 451 8 Gogala, M. *et al.* Structures of the Sec61 complex engaged in nascent peptide translocation or
452 membrane insertion. *Nature* **506**, 107-110 (2014).
- 453 9 Voorhees, R. M. *et al.* Structure of the Sec61 channel opened by a signal sequence. *Science* **351**,
454 88-91 (2016).
- 455 10 Li, L. *et al.* Crystal structure of a substrate-engaged SecY protein-translocation channel. *Nature*
456 **531**, 395-399 (2016).
- 457 11 Itskanov, S. *et al.* Structure of the posttranslational Sec protein-translocation channel complex
458 from yeast. *Science* **363**, 84-87 (2019).
- 459 12 Wu, X. *et al.* Structure of the post-translational protein translocation machinery of the ER
460 membrane. *Nature* **566**, 136-139 (2019).
- 461 13 Itskanov, S. *et al.* Stepwise gating of the Sec61 protein-conducting channel by Sec63 and Sec62.
462 *Nat Struct Mol Biol* **28**, 162-172 (2021).
- 463 14 Weng, T. H. *et al.* Architecture of the active post-translational Sec translocon. *EMBO J* **40**,
464 e105643 (2021).
- 465 15 Pauwels, E. *et al.* Inhibitors of the Sec61 Complex and Novel High Throughput Screening
466 Strategies to Target the Protein Translocation Pathway. *Int J Mol Sci* **22** (2021).
- 467 16 Luesch, H. *et al.* Natural products as modulators of eukaryotic protein secretion. *Nat Prod Rep*
468 **37**, 717-736 (2020).
- 469 17 Guenin-Mace, L. *et al.* Shaping mycolactone for therapeutic use against inflammatory disorders.
470 *Sci Transl Med* **7**, 289ra285 (2015).
- 471 18 Heaton, N. S. *et al.* Targeting Viral Proteostasis Limits Influenza Virus, HIV, and Dengue Virus
472 Infection. *Immunity* **44**, 46-58 (2016).
- 473 19 Vermeire, K. *et al.* CADA inhibits human immunodeficiency virus and human herpesvirus 7
474 replication by down-modulation of the cellular CD4 receptor. *Virology* **302**, 342-353 (2002).
- 475 20 O'Keefe, S. *et al.* Ipomoeassin-F inhibits the in vitro biogenesis of the SARS-CoV-2 spike protein
476 and its host cell membrane receptor. *J Cell Sci* **134** (2021).
- 477 21 Lowe, E. *et al.* Preclinical evaluation of KZR-261, a novel small molecule inhibitor of Sec61.
478 *Journal of Clinical Oncology* **38**, 3582-3582 (2020).
- 479 22 Besemer, J. *et al.* Selective inhibition of cotranslational translocation of vascular cell adhesion
480 molecule 1. *Nature* **436**, 290-293 (2005).

481 23 Garrison, J. L. *et al.* A substrate-specific inhibitor of protein translocation into the endoplasmic
482 reticulum. *Nature* **436**, 285-289 (2005).

483 24 MacKinnon, A. L. *et al.* Photo-leucine incorporation reveals the target of a cyclodepsipeptide
484 inhibitor of cotranslational translocation. *J Am Chem Soc* **129**, 14560-14561 (2007).

485 25 Junne, T. *et al.* Decatransin, a new natural product inhibiting protein translocation at the
486 Sec61/SecYEG translocon. *J Cell Sci* **128**, 1217-1229 (2015).

487 26 Paatero, A. O. *et al.* Apratoxin Kills Cells by Direct Blockade of the Sec61 Protein Translocation
488 Channel. *Cell Chem Biol* **23**, 561-566 (2016).

489 27 McKenna, M. *et al.* Mechanistic insights into the inhibition of Sec61-dependent co- and post-
490 translational translocation by mycolactone. *J Cell Sci* **129**, 1404-1415 (2016).

491 28 Baron, L. *et al.* Mycolactone subverts immunity by selectively blocking the Sec61 translocon. *J*
492 *Exp Med* **213**, 2885-2896 (2016).

493 29 Zong, G. *et al.* Ipomoeassin F Binds Sec61alpha to Inhibit Protein Translocation. *J Am Chem Soc*
494 **141**, 8450-8461 (2019).

495 30 Tranter, D. *et al.* Coibamide A Targets Sec61 to Prevent Biogenesis of Secretory and Membrane
496 Proteins. *ACS Chem Biol* **15**, 2125-2136 (2020).

497 31 Vermeire, K. *et al.* Signal peptide-binding drug as a selective inhibitor of co-translational protein
498 translocation. *PLoS Biol* **12**, e1002011 (2014).

499 32 Cross, B. C. *et al.* Eeyarestatin I inhibits Sec61-mediated protein translocation at the
500 endoplasmic reticulum. *J Cell Sci* **122**, 4393-4400 (2009).

501 33 Pauwels, E. *et al.* A Proteomic Study on the Membrane Protein Fraction of T Cells Confirms High
502 Substrate Selectivity for the ER Translocation Inhibitor Cyclotriazadisulfonamide. *Mol Cell*
503 *Proteomics* **20**, 100144 (2021).

504 34 Mackinnon, A. L. *et al.* An allosteric Sec61 inhibitor traps nascent transmembrane helices at the
505 lateral gate. *Elife* **3**, e01483 (2014).

506 35 Gerard, S. F. *et al.* Structure of the Inhibited State of the Sec Translocon. *Mol Cell* **79**, 406-415
507 e407 (2020).

508 36 Rehan, S. *et al.* Signal peptide mimicry primes Sec61 for client-selective inhibition. *bioRxiv*,
509 2022.2007.2003.498529 (2022).

510 37 Pauwels, E. *et al.* Structural insights into TRAP association with ribosome-Sec61 complex and
511 translocon inhibition by a CADA derivative. *Sci Adv* **9**, eadf0797 (2023).

512 38 Carlson, M. L. *et al.* The Peptidisc, a simple method for stabilizing membrane proteins in
513 detergent-free solution. *Elife* **7** (2018).

514 39 Hommel, U. *et al.* The 3D-structure of a natural inhibitor of cell adhesion molecule expression.
515 *FEBS Lett* **379**, 69-73 (1996).

516 40 Luesch, H. *et al.* Total structure determination of apratoxin A, a potent novel cytotoxin from the
517 marine cyanobacterium *Lyngbya majuscula*. *J Am Chem Soc* **123**, 5418-5423 (2001).

518 41 Trueman, S. F. *et al.* A gating motif in the translocation channel sets the hydrophobicity
519 threshold for signal sequence function. *J Cell Biol* **199**, 907-918 (2012).

520 42 Smith, M. A. *et al.* Modeling the effects of prl mutations on the Escherichia coli SecY complex. *J*
521 *Bacteriol* **187**, 6454-6465 (2005).

522 43 Junne, T. *et al.* Mutations in the Sec61p channel affecting signal sequence recognition and
523 membrane protein topology. *J Biol Chem* **282**, 33201-33209 (2007).

524 44 Klein, W. *et al.* Defining a conformational consensus motif in cotransin-sensitive signal
525 sequences: a proteomic and site-directed mutagenesis study. *PLoS One* **10**, e0120886 (2015).

526 45 Van Puyenbroeck, V. *et al.* Preprotein signature for full susceptibility to the co-translational
527 translocation inhibitor cyclotriazadisulfonamide. *Traffic* **21**, 250-264 (2020).

528 46 Fessl, T. *et al.* Dynamic action of the Sec machinery during initiation, protein translocation and
529 termination. *Elife* **7** (2018).
530 47 Mercier, E. *et al.* Lateral gate dynamics of the bacterial translocon during cotranslational
531 membrane protein insertion. *Proc Natl Acad Sci U S A* **118** (2021).
532 48 Bhadra, P. *et al.* Mycolactone enhances the Ca²⁺ leak from endoplasmic reticulum by trapping
533 Sec61 translocons in a Ca²⁺ permeable state. *Biochem J* **478**, 4005-4024 (2021).
534 49 Gamayun, I. *et al.* Eeyarestatin Compounds Selectively Enhance Sec61-Mediated Ca²⁺ Leakage
535 from the Endoplasmic Reticulum. *Cell Chem Biol* **26**, 571-583 e576 (2019).
536

537 **Methods**

538 **Sec61 Inhibitors**

539 Isolation of cotransin CP2 and decatransin from fungal species have been described
540 previously²⁵. For apratoxin F, ipomoeassin F, and mycolactone, we used synthetic versions.
541 Synthesis of apratoxin F (ref. ⁵⁰), ipomoeassin F (ref. ⁵¹), mycolactone (ref. ⁵²) has been as
542 described previously. We note that apratoxin F and its more commonly studied analog apratoxin
543 A have only a minor structural difference and both are known to exhibit comparable IC₅₀ values
544 on mammalian cancer cell lines⁵⁰. We also note that the used synthetic mycolactone is a 4:1
545 mixture of two epimers at C12 in favor of the natural configuration. CADA and ESI were
546 purchased from Calbiochem (cat# 534337 and 324521, respectively). Inhibitors were dissolved
547 in dimethyl sulfoxide (DMSO) at 10 mM (for decatransin, ipomoeassin F, and mycolactone), 20
548 mM (for cotransin CP2, apratoxin F, and CADA), or 50 mM (for ESI) before use.

549 **Plasmid constructs for cryo-EM studies**

550 The plasmids and yeast strain to express the *S. cerevisiae* Sec complex have been described
551 previously^{11,13}. To express the human Sec complex in *Spodoptera frugiperda* (Sf9) cells, we
552 modified a Bac-to-Bac baculovirus expression vector (Invitrogen) adapting the multigene-
553 expression approach from MoClo Yeast ToolKit (YTK)⁵³ as follows. First, we generated part
554 plasmids for a baculovirus polyhedrin (PH) promoter and a SV40 polyA signal, and an acceptor
555 plasmid (pBTK1) consisting of the backbone of pFastBac-1 (including a Tn7L element, an
556 ampicillin resistance gene, a pUC *E. coli* origin of replication, a Tn7R element and a gentamycin
557 resistance gene) and a *BsmBI*-superfolder GFP (sfGFP)-*BsmBI* acceptor cassette from
558 pYTK096 (ref. ⁵³). Gene fragments encoding human Sec subunits were chemically synthesized
559 and individually cloned into the entry plasmid pYTK001 as coding sequence (CDS) parts. Amino
560 acids sequences of human (denoted by “Hs”) Sec61, Sec62, and Sec63 subunits are from the
561 following entries in UniProt: P61619 (S61A1_HUMAN) for HsSec61 α , P60468
562 (SC61B_HUMAN) for HsSec61 β , P60059 (SC61G_HUMAN) for HsSec61 γ , Q99442
563 (SEC62_HUMAN) for HsSec62, and Q9UGP8 (SEC63_HUMAN) for HsSec63. For the
564 pYTK001-HsSec63 plasmid, a DNA segment encoding a human rhinovirus (HRV) 3C-cleavable
565 linker (amino acid sequence: GAGSNSLEVL \textit{FQGP} TAAAA; *italic*, HRV 3C cleavage site) and an
566 enhanced green fluorescence protein (eGFP) were inserted immediately before the stop codon
567 of HsSec63. To generate single Sec gene expression cassettes, each Sec subunit CDS was
568 assembled with connectors (from pYTK003–007 and pYTK067–072), the PH promoter, and the
569 SV40 terminator into pYTK095 using *BsaI* Golden Gate cloning. Then, all Sec subunit
570 expression cassettes were assembled into pBTK1 using *BsmBI* Golden Gate cloning. In this
571 multigene plasmid, the expression cassettes were arranged in the following order: PH-
572 HsSec61 α -SV40 | PH-HsSec61 γ -SV40 | PH-HsSec61 β -SV40 | PH-HsSec63-3C-eGFP-SV40 |
573 PH-HsSec62-SV40.

574 The plasmid expressing the human-yeast chimeric Sec complex was made similarly to the
575 human Sec complex plasmid with modifications of pYTK95 HsSec61 α and HsSec63 expression
576 constructs as follows. To modify Sec61 α , two substitution mutations were introduced in cytosolic
577 loops of HsSec61 α using PCR to replace (1) amino acid residues 263–278
578 (VDLPIKSARYRGQYNT) with the corresponding yeast sequence (residues 265–280;
579 YELPIRSTKVRGQIGI) and (2) amino acid residues 394–411 (LKEQQMVMRGRHRETSMVH)
580 with amino acids 395–412 of ScSec61 (FKDQGMVINGKRETSIYR;

581 “Sc” denotes *Saccharomyces cerevisiae*). The substitutions in HsSec63 were introduced using
582 Gibson assembly by first substituting amino acid residues 30–96 (ATY...VKK) with amino acids
583 29–93 of ScSec63 (MTL...RRN), followed by substitution of residues 215 to the C-terminus
584 (SIR...stop) with the corresponding sequence from ScSec63 (residues 246–stop; TQS...stop).
585 Fragments of ScSec63 were amplified from genomic DNA of yeast strain BY4741. In the
586 multigene pBTK1 construct of the chimeric Sec complex, HsSec62 cassette was omitted, and
587 instead, the cassettes for ScSec71 (PH-ScSec71-SV40) and ScSec72 (PH-ScSec72-SV40)
588 were added. The CDS fragments of ScSec71 and ScSec72 were amplified by PCR from
589 genomic DNA of yeast strain BY4741 and cloned into pYTK001. Like other single subunit
590 expression plasmids, ScSec71 and ScSec72 CDSs were assembled into pYTK095 together
591 with the PH promoter and the SV40 polyA signal before use for the *BsmBI* assembly.

592 **Protein Expression**

593 Baculovirus bacmids encoding the human or chimeric Sec complex were generated by
594 transforming the respective pBTK1 plasmid into the DH10Bac *E. coli* cells (Invitrogen) according
595 to the manufacturer’s instructions. Bacmids were isolated using a DNA midiprep kit (Epoch Life
596 Science). 40 mL of a Sf9 suspension culture were prepared in ESF921 medium (Expression
597 Systems) to a density of ~1.5 M/mL. 40 µg bacmid DNA were mixed with 80 µg PEI Max
598 transfection reagent (PolySciences) in 4 mL Dulbecco’s phosphate-buffered saline (DPBS).
599 After incubating at 22°C for 20–30 minutes, the DNA:PEI mixture was added to the culture.
600 Supernatant containing P1 virus was harvested ~4 days post transfection and stored at 4°C
601 after supplementing 5% FBS (Gibco). Expression of the Sec complex was carried out by adding
602 0.5 mL P1 virus to 0.7 L of Sf9 cells at density of ~1.5 M/ml that were prepared in a 2-L baffled
603 flask. Cells were harvested by centrifugation typically two to three days post-infection upon
604 verifying uniform expression of green fluorescence under microscope. Cell pellets were frozen
605 in liquid nitrogen and stored at –80°C until use.

606 **Protein Purification**

607 The yeast Sec complex was purified from yeast strain ySI8 (ref. ¹³). This strain expresses a
608 “pore mutant (PM)” version of ScSec61, the pore ring residues of which were mutated to amino
609 acids corresponding to HsSec61α (M90L/T185I/M294I/M450L). The yeast Sec complex was
610 purified as described previously^{11,13}. After Superose 6 (GE Life Sciences) size-exclusion
611 chromatography, the purified protein was concentrated to ~4 mg/mL in 20 mM Tris pH 7.5, 100
612 mM NaCl, 1mM EDTA, 2 mM DTT, and 0.02% glycol-diosgenin (GDN; Anatrace) and mixed
613 with 100 µM cotransin CP2 for 0.5–1 h before preparing cryo-EM grids.

614 To purify the human Sec complexes, Sf9 cell pellets were first resuspended in lysis buffer
615 containing 50 mM Tris-HCl pH 7.5, 200 mM NaCl, 2 mM dithiothreitol (DTT), 1 mM
616 ethylenediaminetetraacetic acid (ETDA) supplemented with protease inhibitors (5 µg/ml
617 aprotinin, 5 µg/ml leupeptin, 1 µg/ml pepstatin A, and 1.2 mM PMSF). All subsequent steps
618 were carried out in ice or at 4°C. The cells were broken with a glass Dounce homogenizer using
619 ~100 strokes. After removing large debris by brief centrifugation (4,000 g, 10 min), membranes
620 were pelleted by ultracentrifugation for 1.5 h (125,000 g, Beckman Type 45 Ti). The membrane
621 pellet was resuspended in ~10 pellet volumes of lysis buffer supplemented with 5 µM cotransin
622 CP2. Membranes were solubilized by an addition of 1% lauryl maltose neopentyl glycol (LMNG;
623 Anatrace) and 0.2% cholesteryl hemisuccinate (CHS; Anatrace) for 2 h. Then, the lysate was
624 clarified by ultracentrifugation at 125,000 g for 1 h. The clarified lysate was then supplemented

625 with 2 μg *Serratia marcescens* nuclease and incubated with home-made anti-GFP nanobody
626 Sepharose beads for 1.5 h. Beads were washed with wash buffer containing 25 mM Tris-HCl pH
627 7.5, 100 mM NaCl, 2 mM DTT, 1 mM EDTA, 0.02% GDN, and 5 μM cotransin CP2 (hereafter, 5
628 μM cotransin CP2 was included in all buffers). The complex was eluted by incubating beads
629 with the HRV 3C protease overnight. The eluate was collected and concentrated to ~ 10 mg/ml
630 by Amicon Ultra (cutoff 100 kDa). The sample was then injected to a Superose 6 increase
631 column (GE Life Sciences) equilibrated with the wash buffer. Peak fractions were pooled and
632 concentrated to ~ 6 mg/mg, before preparing cryo-EM grids.

633 The chimeric Sec complex was purified similarly using the method to purify the human Sec
634 complex but with minor modifications. First, the Sec complex was purified without
635 supplementing Sec61 inhibitors during purification (inhibitors were added to the purified Sec
636 complex before cryo-EM grid preparation). Second, to solubilize membranes, 1% n-dodecyl- β -
637 D-maltopyranoside (DDM; Anatrace) and 0.2% CHS was used instead of LMNG/CHS. For
638 column wash, the buffer contained 0.02% DDM and 0.004% CHS instead of GDN. Third, the
639 Sec complex was reconstituted into a peptidisc³⁸ as follows. After concentrating the eluate from
640 GFP-nanobody beads to ~ 10 mg/ml, the Sec complex was mixed with the peptidisc protein
641 (Peptidisc Lab) at a weight ratio of 1.5:1 (peptidisc to Sec). After incubating for 1 h, the mixture
642 was injected into a Superose 6 Increase column equilibrated with 25 mM Tris-HCl pH 7.5, 100
643 mM NaCl, 2 mM DTT and 1 mM EDTA. Peak fractions were pooled and concentrated to ~ 10
644 mg/ml, and one of the Sec61 inhibitors was added for ~ 1 h before preparing cryo-EM grids. The
645 inhibitor concentrations used were: 100 μM for cotransin CP2, 100 μM for decatransin, 100 μM
646 for apratoxin F, 100 μM for ipomoeassin F, 100 μM for mycolactone, 200 μM for CADA, and 500
647 μM for ESI. These concentrations, except for that of ESI, correspond to a 2–4-fold molar excess
648 to the protein concentration (~ 52 μM) to ensure saturated binding. A higher concentration was
649 used for ESI based on a relatively low (70 μM) IC_{50} reported in an in-vitro experiment³².

650 **Cryo-EM data acquisition**

651 Immediately prior to preparing cryo-EM grids, 3 μM Fos-Choline-8 (Anatrace) was added to the
652 protein sample. The sample was then applied to a gold Quantifoil R 1.2/1.3 holey carbon grid
653 (Quantifoil) that was glow discharged for 35 sec using PELCO easiGlow glow discharge
654 cleaner. The grid was blotted for 3–4 sec using Whatman No. 1 filter paper and plunge frozen
655 using Vitrobot Mark IV (FEI) set at 4°C and 100% humidity.

656 The yeast Sec complex dataset (1,578 movies) was acquired on FEI Talos Arctica electron
657 microscope operated at an acceleration voltage of 200 kV, with Gatan K2 Summit direct
658 electron detector. A magnification of 36,000x under super resolution mode (with the physical
659 pixel size of 1.14 Å) was used with a nominal defocus range that was set between -0.8 to -2.2
660 μm . Each micrograph was composed of 42 frames with total exposure of 50 e^-/pixel .

661 The human Sec complex dataset (3,499 movies) was collected on FEI Titan Krios G2
662 microscope operating at an acceleration voltage of 300 kV and equipped with a Gatan Quantum
663 Image Filter (slit width of 20 eV) and a Gatan K3 direct electron detector. A magnification of
664 64,000x under the super-resolution mode (with physical pixel size of 0.91 Å) was used at a
665 defocus range that was set between -0.8 and -2.0 . Each micrograph was composed of 42
666 frames with total exposure of 50 e^-/pixel . Exposures were performed with beam shifts onto 9
667 holes (3 by 3) per stage movement.

668 All chimeric Sec complex datasets were acquired on an FEI Titan Krios G3i electron microscope
669 operating at an acceleration voltage of 300 kV, with a Gatan K3 Summit direct electron detector
670 and a Gatan Quantum Image Filter (with 20 eV slit width). A magnification of 81,000x under the
671 super-resolution mode (with physical pixel size of 1.05 Å) was used at a defocus range that was
672 set between -0.8 and -2.0. Each micrograph was composed of 50 frames with a total exposure
673 of 50 e⁻/pixel. Exposures were performed with beam shifts onto 9 holes (3 by 3) per stage
674 movement (often acquiring movies for two non-overlapping areas per hole). All datasets were
675 acquired using SerialEM software⁵⁴.

676 **Cryo-EM image analysis**

677 Preprocessing of the movies and particle image extraction were done using Warp⁵⁵. Motion
678 correction and CTF estimation were performed on images divided to 7 × 5 tiles, and particles
679 (256 x 256 pixels) were picked by the BoxNet algorithm in Warp. All subsequent image
680 processing procedures were performed using cryoSPARC v3.3 (ref. ⁵⁶).

681 Cotransin CP2-treated pore mutant ScSec complex: A data processing flowchart diagram is
682 shown in [Extended Data Fig. 1a](#). A dataset of 528,128 auto-picked particles was classified into
683 fifty 2-D class averages. Using visual inspection of the output, classes that represented empty
684 micelles or poor-quality classes were removed and particles grouped into well-resolved classes
685 corresponding to a single copy of the full Sec complex were selected (385,686 particles). Three
686 ab-initio 3-D maps were then generated in cryoSPARC using the selected particles, followed by
687 heterogeneous refinement. One 3-D class with 274,913 particles refined to a density map
688 exhibiting defined Sec complex features. Non-uniform refinement of the particles in this class
689 yielded a consensus map with 3.9-Å overall resolution. The particles were further separated into
690 two 3-D classes using a heterogeneous refinement with inputs of the consensus map and the
691 consensus map with manually erased Sec62. After a subsequent round of non-uniform
692 refinement 174,058 particles yielded a map of ScScSec complex with Sec62 at 4.0-Å overall
693 resolution, and 100,855 particles yielded a map of ScSec complex without Sec62 at 4.2-Å
694 overall resolution.

695 Cotransin CP2-bound wildtype HsSec complex: A data processing flowchart diagram is shown
696 in [Extended Data Fig. 1d](#). A dataset of 601,465 auto-picked particles was classified into seventy
697 2-D class averages. Selected classes yielded 330,005 particles that were then reconstructed
698 into three 3-D classes using ab-initio reconstruction followed by heterogeneous refinement. One
699 major class, with 202,946 particles, was selected for further refinement. Non-uniform refinement
700 of this class resulted in a reconstruction only at 7.4-Å resolution due to poor image alignment.
701 Thus, for the final map, we used the ab-initio reconstruction method (without splitting the particle
702 sets for half maps) with the maximal refinement resolution manually set to 5.0-Å ([Extended Data](#)
703 [Fig. 1f](#)).

704 Apo chimeric Sec complex: A data processing flowchart diagram is shown in [Extended Data](#)
705 [Fig. 2b](#). Using 2-D classifications starting with 616,121 auto-picked particles, we selected
706 363,027 particles for 3-D reconstruction. Following an ab-initio refinement step generating four
707 initial maps and a heterogeneous refinement step we identified two major 3-D classes with
708 distinguishable full Sec complex features. Each of these classes were refined using non-uniform
709 refinement, local CTF refinement, and another round of non-uniform refinement, yielding full
710 maps of the chimeric Sec complex at overall resolutions of 2.7 and 2.8 Å from 188,637 particles
711 (Class 1) and 147,081 particles (Class 2), respectively. The Sec61 channel was further refined

712 by masking out the cytosolic domains of the complex and performing local refinement, yielding
713 overall channel resolutions of 3.0 Å (Class 1) and 3.4 Å (Class 2).

714 Apratoxin F-bound chimeric Sec complex: A data processing flowchart diagram is shown in
715 [Extended Data Fig. 3b](#). Using 2-D classifications starting with 910,463 auto-picked particles, we
716 selected 534,411 particles for 3-D reconstruction. Following an ab-initio refinement step
717 generating four initial maps and a heterogeneous refinement step we identified two structurally
718 indistinguishable major 3-D classes with defined full Sec complex features. The particles from
719 the two classes were combined and refined using non-uniform refinement, local CTF
720 refinement, and another round of non-uniform refinement, yielding a full map of the apratoxin F
721 bound chimeric Sec complex at an overall resolution of 2.5 Å from 497,555 particles. The Sec61
722 channel was further refined by masking out the cytosolic domains of the complex and
723 performing local refinement, producing an overall channel resolution of 2.6 Å.

724 All other inhibitor-bound datasets were processed using a workflow described for Apratoxin F-
725 bound structure with minor variations in the numbers of classes in 2-D and 3-D classification
726 procedures. For details, see [Supplementary Information Figs. 1 and 2](#). Statistics for final refined
727 maps are shown in [Extended Data Fig. 4 and Supplementary Tables 1 and 2](#).

728 **Model building and refinement**

729 Atomic model building and refinement were performed using Coot (version 0.9.8.1)⁵⁷ and
730 Phenix (version 1.19.2)⁵⁸. An initial model was built by docking an ScSec complex model (PDB
731 ID 7KAH; ref. ¹³) into the cryo-EM map of the cotransin CP2-bound complex using UCSF
732 chimera (version 1.16)⁵⁹ and rebuilding the polypeptide chains. For building and refining of
733 Sec61 and inhibitor models, we used maps from focused (local) refinements as they typically
734 showed better protein side-chain and inhibitor features than full maps. The initial model was
735 further improved by using our highest-resolution map, which was obtained from the apratoxin F-
736 bound complex. This model was then used to build atomic models for apo and other inhibitor-
737 bound complexes by docking the model to the map using UCSF Chimera and locally adjusting it
738 into the map in Coot. The restraint models of inhibitors were generated from SMILES strings of
739 inhibitors using the Grade web server (<http://grade.globalphasing.org>) or the eLBOW tool of
740 Phenix. The atomic models of inhibitors were then fitted into the cryo-EM map in Coot. We note
741 that stereochemistry of decatransin has not been experimentally determined. We assumed that
742 all amino acid residues of decatransin are in an L or S configuration based on an observation
743 that no epimerase was found in the biosynthetic gene cluster of decatransin. The configuration
744 of C α of the homoleucine-derived 2-hydroxy carboxylic acid remains ambiguous²⁵, but we also
745 assumed that it is in an S configuration. The resulting model could be fitted well into the cryo-
746 EM map. The atomic models were refined with Phenix real-space refinement using maps that
747 were sharpened with B-factors estimated based on the Guinier plots and low-pass-filtered at
748 their overall resolution. The refinement resolution was also limited to the overall resolution of the
749 maps in Phenix. Structural validation was performed using MolProbity included in the Phenix
750 package. UCSF Chimera, ChimeraX (version 1.4), and PyMOL (version 2.5.1; Schrödinger)
751 were used to prepare figures in the paper.

752 **Mutagenesis of yeast Sec61 α and IC₅₀ measurements**

753 Except for the experiment shown in Fig. 4c, cotransin CP2 IC₅₀ measurements were based on
754 the yeast strain RSY1293 (*mata*, *ura3-1*, *leu2-3,-112*, *his3-11,-15*, *trp1-1*, *ade2-1*, *can1-*
755 *100*, *sec61::HIS3*, [pDQ1]) (ref. ⁶⁰). In strain RSY1293URA, pDQ1, i.e., YCplac111 (*LEU2 CEN*)

756 containing the gene of an N-terminally His-tagged, otherwise wild-type Sec61 α (Sec61p) with its
757 own promoter, was exchanged for YCplac33 (*URA3 CEN*) containing the same insert. Mutations
758 in *sec61* were introduced in pDQ1 by PCR and transformed into RSY1293URA, followed by
759 elimination of the *URA3* plasmid containing wild-type using 5-fluoro-orotic acid. Finally, the
760 presence of the mutation was confirmed by sequencing.

761 For experiments shown in Fig. 4 c–e and ipomoeassin IC₅₀ measurements, we used the yeast
762 strain BY4743 Δ 8a (*mat a, ura3 Δ 0, leu2 Δ 0, his3 Δ 1, lys2 Δ 0, snq2::KanMX4; pdr3::KanMX4;*
763 *pdr5::KanMX4; pdr1::NAT1; yap1::NAT1; pdr2 Δ ; yrm1 Δ ; yor1 Δ) lacking eight genes involved in
764 drug resistance (efflux pumps *SNQ2*, *PDR5*, and *YOR1*, and transcription factors *PDR1*, *PDR2*,
765 *PDR3*, *YAP1*, and *YRM1*)⁶¹. This strain showed higher sensitivity to ipomoeassin F compared to
766 RSY1293. YCplac33 containing (untagged) *SEC61* with 200 bp of its own upstream and 205 bp
767 of its own downstream sequence was transformed into BY4743 Δ 8a. Genomic *SEC61* together
768 with 194 bp 5'- and 204 bp 3'-noncoding sequence was replaced with a hygromycin resistance
769 cassette using pAG32 (*HphMX4*) resulting in the strain BY4743 Δ 9aURA (*sec61::HphMX4*
770 [pSEC61-YCplac33]). Finally, pDQ1 containing the mutated *sec61* versions were transformed
771 and the wild-type *SEC61* URA3 plasmid counterselected. Plasmid exchange was validated by
772 PCR. The IC₅₀ measurements for cotransin CP2 in the BY4743 Δ 9aURA background paralleled
773 those in the RSY1293.*

774 IC₅₀ measurements were performed as described previously²⁵ by testing log-phase cultures in
775 96-well microtiter plates in YPD medium with serial dilutions of the compound. The assay
776 volume was 120 μ l/well, start OD₆₀₀ was 0.05, DMSO was normalized to 2%. Curves were
777 calculated by taking the 19 h OD₆₀₀ measurements and applying a log regression curve fit in
778 TIBCO Spotfire (version 3.2.1).

779 **Preparation of stable mammalian cell lines**

780 A DNA segment encoding human SEC61A1 was synthesized and cloned into pcDNA5/FRT/TO
781 (Life Technologies) followed by addition of a C-terminal HA-tag, an internal ribosome entry site
782 (IRES), and enhanced green fluorescence protein (EGFP) sequences. Point mutants of
783 SEC61A1 were generated by PCR. All cell lines were maintained in DMEM supplemented with
784 10% FBS, 1% Penicillin/Streptomycin (Gibco), and 15 μ g/mL blasticidin S (Gold Biotechnology).
785 In a 6-well dish, Flp-In™ T-REx™-293 cells (Invitrogen, Cat. # R78007) were plated at a density
786 of 5 x 10⁵ cells/well overnight at 37 °C. Plasmids pcDNA5/FRT/TO-SEC61A1-HA-IRES-GFP
787 and pOG44 were co-transfected at a 3:1 ratio with Lipofectamine 3000 (Thermo Fisher, Cat. #
788 L3000001). The next day, media was replaced. After another 24h, cells were transferred to a
789 10cm dish containing fresh DMEM with 15 μ g/mL blasticidin S and 50 μ g/mL Hygromycin B
790 (Gold Biotechnology). Cells were continually monitored with media replacement until several
791 1mm cell colonies became visible (about 3 weeks). Cells were then dissociated and expanded
792 into new 10-cm dishes for cell maintenance. All cell lines were sequence verified by PCR using
793 primers (forward: AAA GTG CTG TGG ACC GCT ATC, reverse: CC AAC TGG ATA AGC ACG
794 TGC TG) specific to the synthetic human *SEC61A1* coding sequence prior to use.

795 **HEK293 viability assay**

796 SEC61A1-overexpressing Flp-In T-Rex-293 cells were seeded in 96-well flat-bottom plates at 5
797 x 10³ cells/well in media containing 1 μ g/mL doxycycline overnight at 37°C. The following day,
798 serial dilutions of compounds were performed in doxycycline-supplemented DMEM media, and

799 cells were treated with compound dilutions for a total incubation volume of 150 μ L (0.11%
800 DMSO v/v). After 72-h incubation, cell viability was measured by addition of 15 μ L resazurin
801 reagent (Biotium, Cat. #30025-1). The plate was incubated for 2 h at 37°C and fluorescence
802 intensity read using a BMG Labtech CLARIOstar plate reader (fluorescence Intensity, excitation
803 at 545 nm and emission at 600nm). The data were processed with Excel, and the curves were
804 generated using R software (version 4.0.5) and *ggplot2* (version 3.3.3) and *drc* (version 3.0-
805 1packages).

806

807 **Human CD4 expression assay**

808 A plasmid expressing a full-length human CD4 cDNA construct under a cytomegalovirus (CMV)
809 promoter (Horizon Discovery, Cat. #MHS6278-202801784) was purchased. An additional single
810 Ser-Gly linker and Strep-tag was appended the C-terminus to the CD4 coding sequence,
811 resulting in pCMV-huCD4-Strep. SEC61A1-overexpressing Flp-In T-Rex-293 cells were seeded
812 in a 12-well plate at 4×10^5 cells/well and pretreated with 1 μ g/ mL doxycycline overnight at
813 37°C. Cells were transfected with pCMV-huCD4-Strep using Lipofectamine LTX (Invitrogen,
814 Cat. #15338030) according to manufacturer protocol. After 6 h, the cells were treated with
815 dilutions of CADA (0.25% DMSO v/v). At 24 h post-treatment, cells were harvested by pipetting,
816 washed with 500 μ L PBS, then lysed directly on ice (50 mM Tris pH 6.8, 2% SDS, 6% glycerol,
817 supplemented with 5 μ g/mL aprotinin, 5 μ g/mL leupeptin, 1 μ g/mL pepstatin A, 1 mM PMSF, and
818 2 μ g/mL Benzonase nuclease). Lysates were then clarified by spinning for 10 min at 17,000g.
819 Protein concentrations were measured by a BCA assay (Thermo Scientific, Cat. #23227) before
820 preparation of samples in SDS-PAGE sample loading buffer. Lysates were separated on 10%
821 Bis-Tris gels (10 μ g/well), transferred to PVDF membranes. Immunoblotting was performed
822 using antibodies against Strep-tag (Genscript, Cat. #A01732; 1:2000), HA-tag (Cell Signaling
823 Technology, Cat. #C29F4, 1:1000), and human SEC61A1 (Cell Signaling Technology, Cat.
824 #D7Q6V, 1:1000). Band intensities were quantified by ImageJ. The data were processed with
825 Excel, and the curves were generated using R software and *ggplot2* and *drc* packages.

826

827 **Data availability**

828 EM maps and models are available through EM Data Bank (EMDB) and Protein Data Bank
829 (PDB) under the following accession codes: EMD-27581 and PDB-8DNL for the apo class 1
830 structure, EMD-27582 and PDB-8DNW for the apo class 2 structure, EMD-27583 and PDB-
831 8DNX for the cotransin CP2-bound complex, EMD-27584 and PDB-8DNY for the decatransin-
832 bound complex, EMD-27585 and PDB-8DNZ for the apratoxin-F-bound complex, EMD-27586
833 and PDB-8DO0 for the mycolactone bound complex, EMD-27587 and PDB-8DO1 for
834 ipomoeassin-F-bound complex, EMD-27588 and PDB-8DO2 for the CADA-bound complex, and
835 EMD-27589 and PDB-8DO3 for the eeyarestatin-I-bound complex. Additional full Sec complex
836 maps were also deposited to EMDB (see [Supplementary Table 1 for accession codes](#)).

837

838 **Methods-only references**

839

840 50 Xiao, L. *Synthetic Apratoxin F and Novel Analogues - Molecules for Anticancer Mechanistic and*
841 *Therapeutic Applications*, The Ohio State University, (2017).

842 51 Zong, G. *et al.* Total Synthesis and Biological Evaluation of Ipomoeassin F and Its Unnatural 11R-
843 Epimer. *J Org Chem* **80**, 9279-9291 (2015).

844 52 Chany, A. C. *et al.* A diverted total synthesis of mycolactone analogues: an insight into Buruli
845 ulcer toxins. *Chemistry* **17**, 14413-14419 (2011).

846 53 Lee, M. E. *et al.* A Highly Characterized Yeast Toolkit for Modular, Multipart Assembly. *ACS Synth*
847 *Biol* **4**, 975-986 (2015).

848 54 Mastronarde, D. N. Automated electron microscope tomography using robust prediction of
849 specimen movements. *J Struct Biol* **152**, 36-51 (2005).

850 55 Tegunov, D. *et al.* Real-time cryo-electron microscopy data preprocessing with Warp. *Nat*
851 *Methods* **16**, 1146-1152 (2019).

852 56 Punjani, A. *et al.* cryoSPARC: algorithms for rapid unsupervised cryo-EM structure
853 determination. *Nat Methods* **14**, 290-296 (2017).

854 57 Emsley, P. *et al.* Features and development of Coot. *Acta Crystallogr D Biol Crystallogr* **66**, 486-
855 501 (2010).

856 58 Afonine, P. V. *et al.* Real-space refinement in PHENIX for cryo-EM and crystallography. *Acta*
857 *Crystallogr D Struct Biol* **74**, 531-544 (2018).

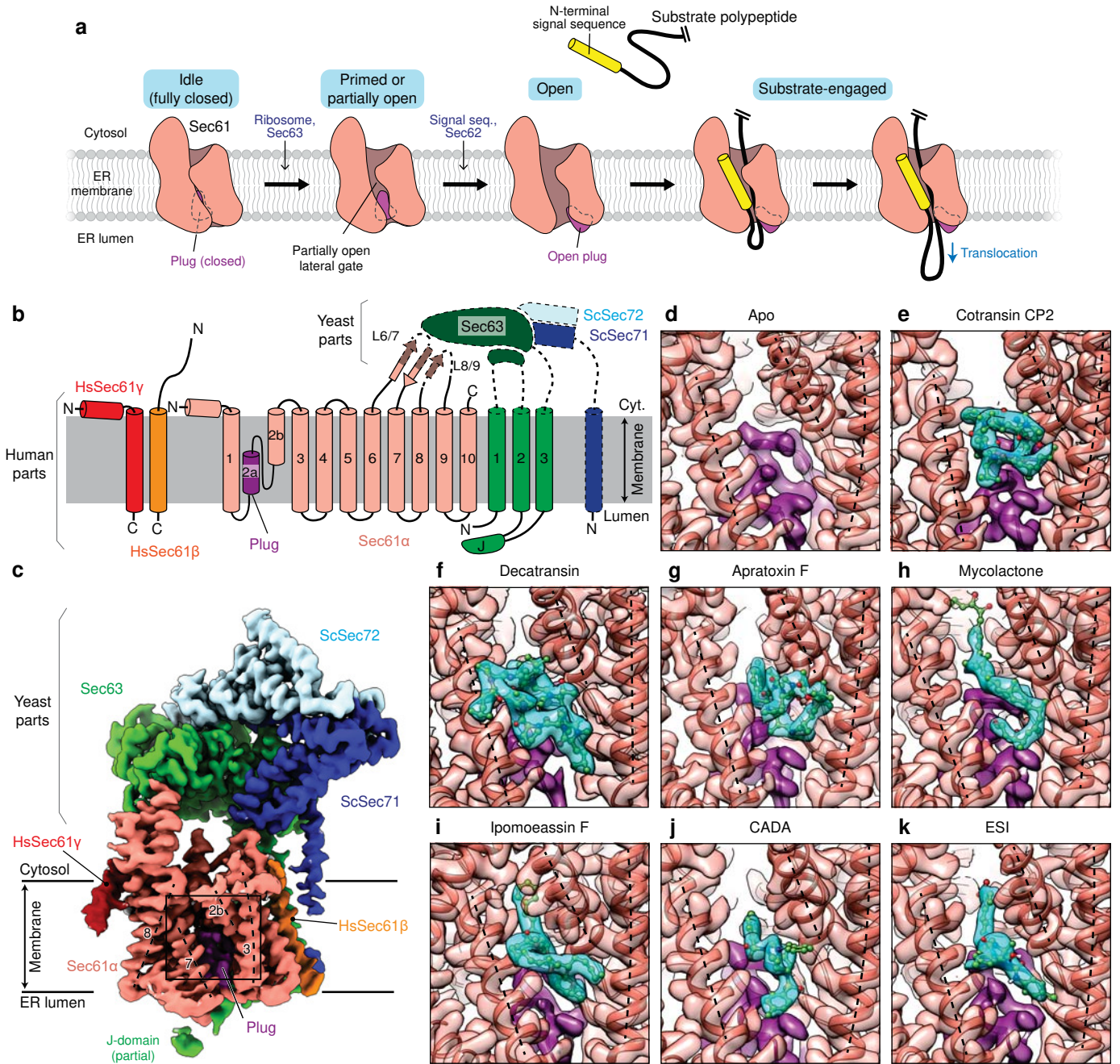
858 59 Pettersen, E. F. *et al.* UCSF Chimera--a visualization system for exploratory research and analysis.
859 *J Comput Chem* **25**, 1605-1612 (2004).

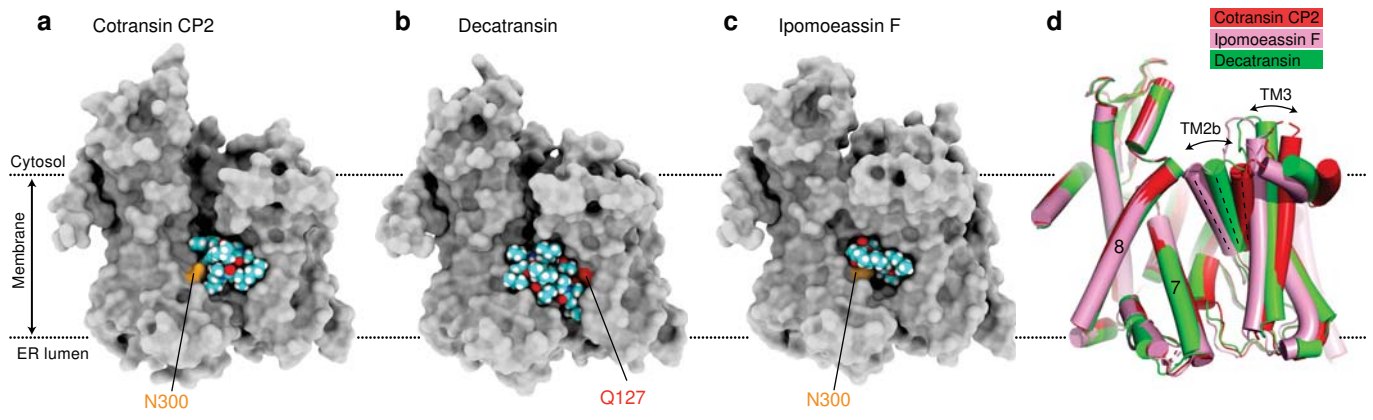
860 60 Pilon, M. *et al.* Sec61p mediates export of a misfolded secretory protein from the endoplasmic
861 reticulum to the cytosol for degradation. *EMBO J* **16**, 4540-4548 (1997).

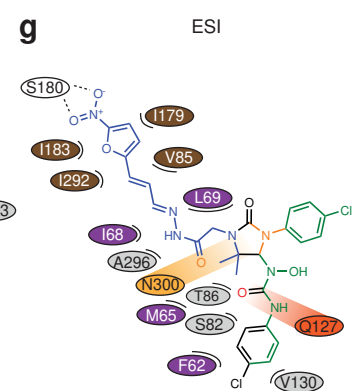
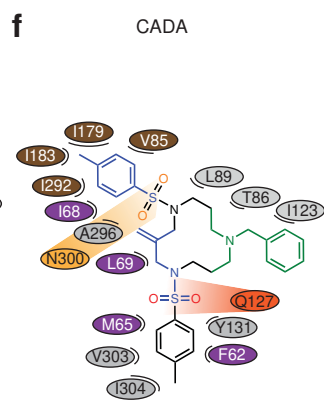
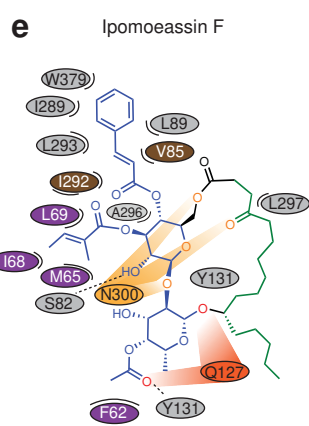
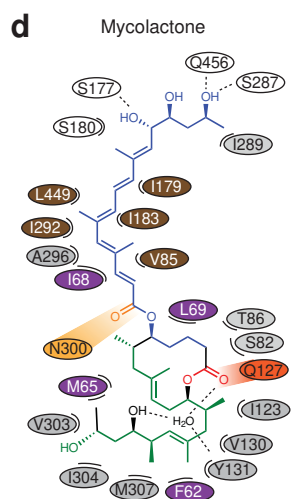
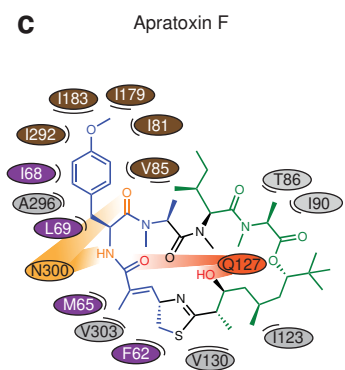
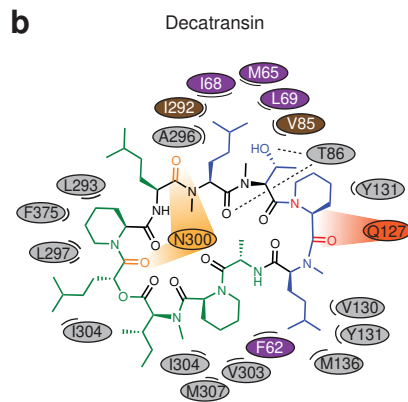
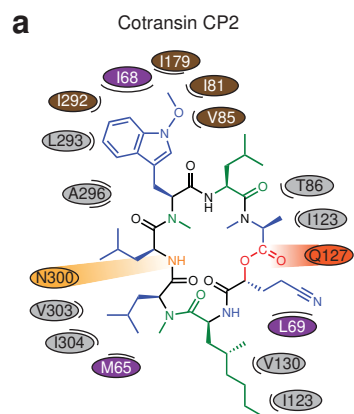
862 61 Hoepfner, D. *et al.* Selective and specific inhibition of the plasmodium falciparum lysyl-tRNA
863 synthetase by the fungal secondary metabolite cladosporin. *Cell Host Microbe* **11**, 654-663
864 (2012).

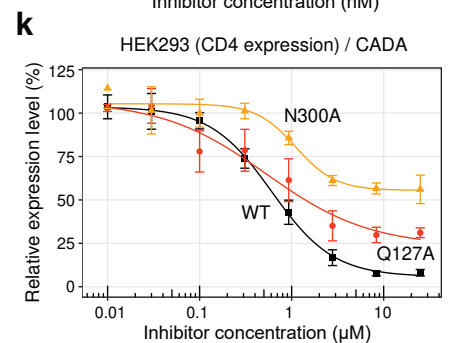
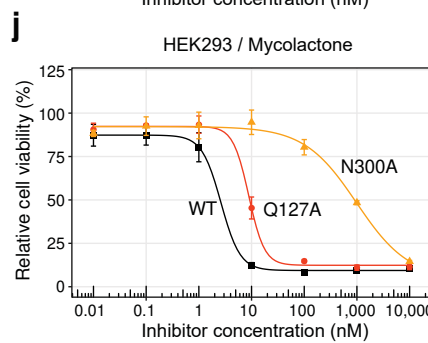
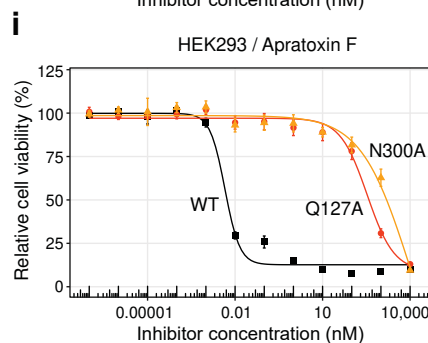
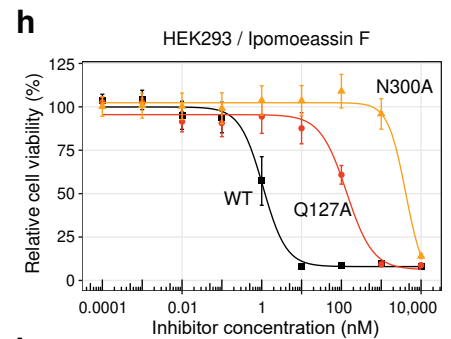
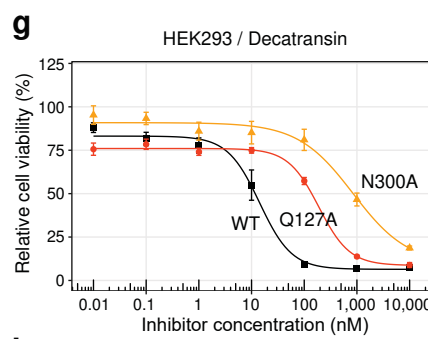
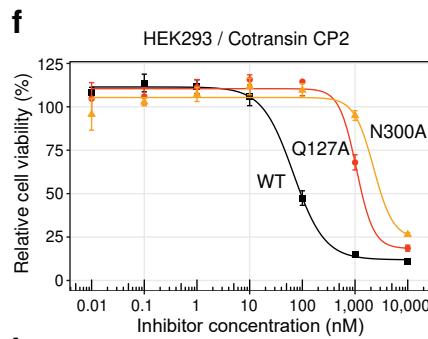
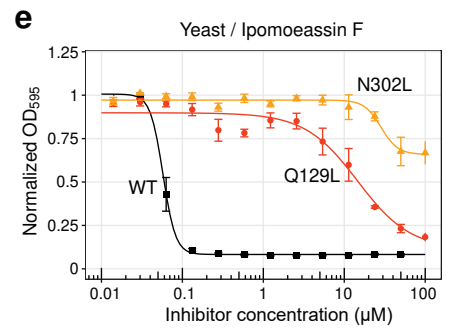
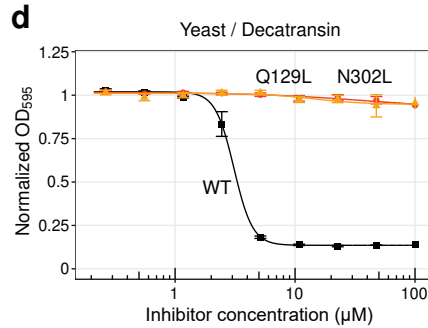
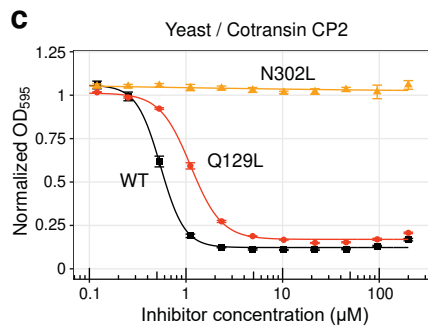
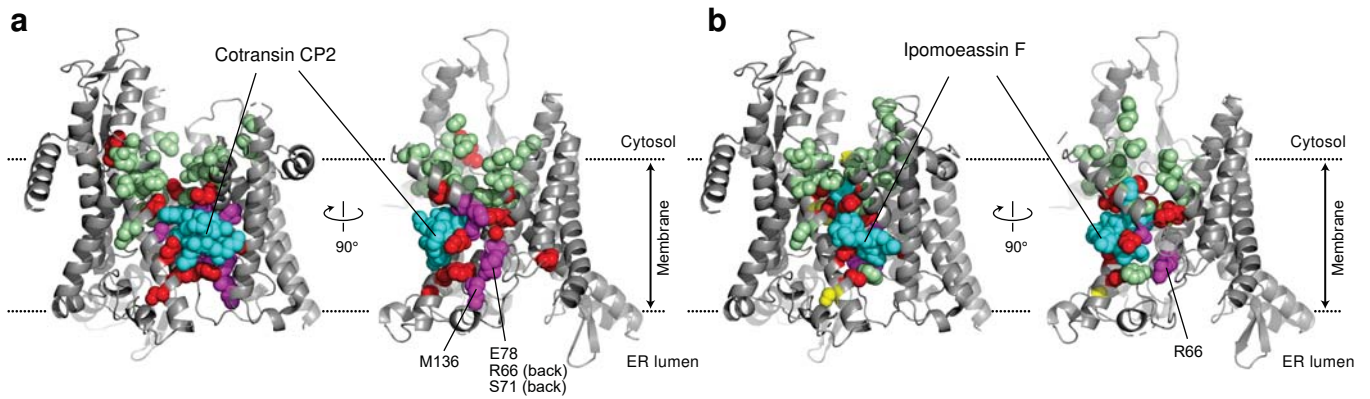
865

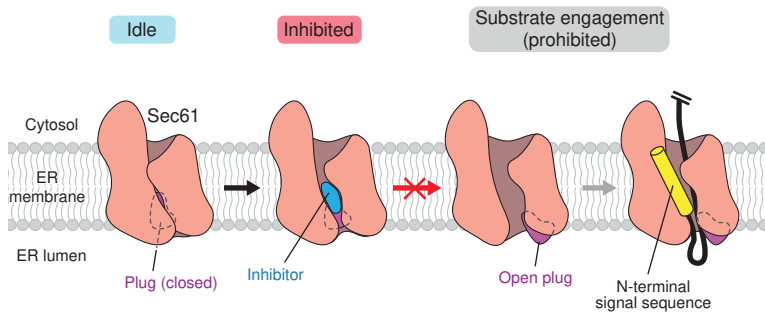
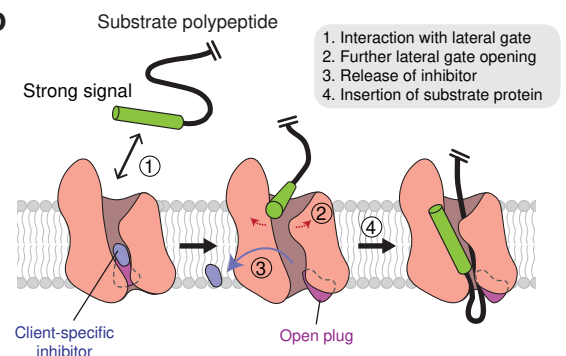
866









a**b**

**Small-molecule inhibitors of
human Sec61 channel *in action***

